CIRP Annals - Manufacturing Technology 00 (2021) 1–4

Contents lists available at ScienceDirect

CIRP Annals - Manufacturing Technology

journal homepage: https://www.editorialmanager.com/CIRP/default.aspx

Graded structures by multi-material mixing in laser powder bed fusion

Wessel W. Wits (2)[a,*], Emiel Amsterdam[b]

[a] Mechanical & Electrical Engineering Department, Thales Nederland B.V., Hengelo, the Netherlands
[b] NLR - Netherlands Aerospace Centre, Marknesse, the Netherlands

A R T I C L E I N F O

Article history:
Available online xxx

Keywords:
Additive manufacturing
Selective Laser Melting (SLM)
Material mixing

A B S T R A C T

Multi-material mixing in laser powder bed fusion is demonstrated by fabricating functionally graded structures in which Inconel and stainless steel are metallurgically bonded. Material mixing and elemental diffusion in the transition zone are studied for single scan tracks, hatch scans and multi-layer builds. An adapted recoater enabling powder deposition from multiple sources was utilized to fabricate a more gradual transition zone by alternating material deposition within the build. Homogenization heat treatment enhances elemental diffusion compared to the as-built configuration resulting in a gradual material transition without a distinct interface. Finally, a multi-material heat exchanger is presented as exemplary design implementation.

1. Introduction

Laser Powder Bed Fusion (LPBF) is one of the most common Additive Manufacturing (AM) processes due to its capability of fabricating fully dense metal parts with complex geometric features [1,2]. However, currently only a limited range of materials is known to process well and new materials development is an active research area driving much of the academic contributions to the literature [3,4]. In this paper, we address novel multi-material processing focusing on the interface between material types and discuss material mixing and elemental diffusion.

Driven by emergent applications in several sectors, there is a need to create multi-material systems with performance improvements in user-defined locations [5]. For LPBF, two distinct approaches of multi-material handling are possible i) a priori material mixing of powder feedstock or ii) in process material mixing during powder deposition of the powder bed. For example, Wits et al. demonstrated LPBF processing of a metal matrix composite using magnesium and silicon carbide as pre-blended feedstock material [6], while Demir and Previtali fabricated parts composed of Fe and Al-12Si by on-demand in-process mixing both constituent materials during layer deposition of the transition layers [7]. In both cases, however, the completion of a structural component was not demonstrated.

Although experimental work on material mixing within the melt pool has been reported, understanding the underlying physics remains challenging due to the difficulties of experimental observation [8]. Also, the order of material deposition has an impact on the interface, as reported by Bai et al. in their attempt to mix steel and bronze [9]. Recently, in 2021, Tan et al. showed that for iron-based multi materials strong metallurgical bonding by phase migration depends on Marangoni flow effects to mix the materials within the melt pool and marked elemental inter-diffusion [10].

* Corresponding author.
E-mail address: wessel.wits@nl.thalesgroup.com (W.W. Wits).

https://doi.org/10.1016/j.cirp.2021.03.005

Koopmann et al. have shown that LPBF can be used to fabricate a multi-material structure made from metal and ceramic by alternating layers of material during a build [11]. However, only one material was used in the machine at a given time and in-process cleaning and refilling was required. In this paper, the machine design was adapted for this study and enabled powder deposition from multiple sources by a multi-material recoater allowing for swift (two-way) material switching.

This study reports on successful mixing of two compatible alloys, Inconel 718 (IN718) and stainless steel 316 L (SS316L) using the apparatus detailed in Fig. 1. The transition zone between both materials is formed by in-process sequential layer deposition using the adapted multi-material recoater. Previous work by Zhou et al. [12], Mei et al. [13]. and Chen et al. [14] have addressed this material system as well for LPBF. Properties of metallurgical bonding and elemental diffusion were reported. Fabricated builds however suffered from (thermal) cracking and porosity near the material interface.

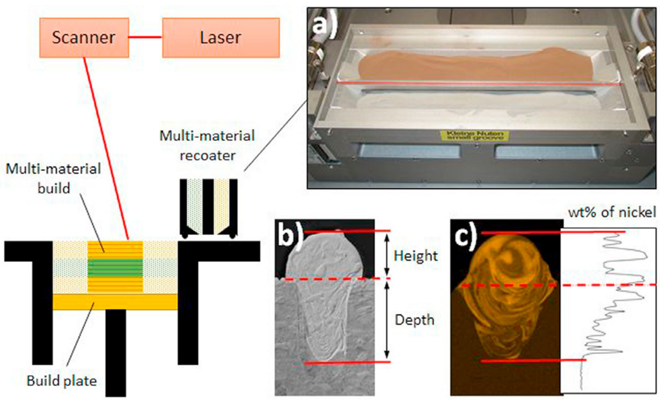

Fig. 1. Schematic image of laser powder bed fusion with adapted recoater for multi-material deposition; inset photograph shows the adapted recoater (a) and micrographs show observation techniques used: melt pool characteristics by optical microscopy (b), and material mixing and elemental diffusion tracked by SEM and EDX (c).

2. Methodology

Specimens were built using an SLM Solutions 280HL system using argon as a shielding gas. A redesigned recoater was used that could handle and deposit two feedstock materials alternatingly, see Fig. 1(a). Commercially available IN718 and SS316L feedstock powders were used of which process parameters are known and widely reported for single-material builds. For the multi-material builds laser power, scan velocity and layer rescanning were systematically varied with the aim of studying melt pool material mixing and elemental diffusion.

Cross-sectional analysis by optical microscopy and Scanning Electron Microscopy (SEM) was performed to determine the size of the melt pool. Alloy mixing within the melt pool was quantified by energy-dispersive X-ray (EDX) analysis and tracking distinct elements such as iron and nickel, see micrographs in Fig. 1(b and c).

To understand melt pool material mixing, single scan tracks were fabricated. Both IN718 feedstock powder was deposited and processed on a SS316L build plate, as well as SS316L feedstock powder on an IN718 build plate. The initial powder layer was 100 µm thick. The material interface and metallurgical bonding were examined by fabricating ten-lines hatch scans with a hatch distance of 120 µm in one deposited layer. Both orders of material deposition were tested. Layer-to-layer penetration and multi-layer elemental diffusion were examined by fabricating a ten-layer build of IN718 feedstock powder on a SS316L build plate. For each new powder layer, the build plate was lowered 50 µm.

A gradual material transition was studied by in-process alternating deposited material layers in the transition zone using the adapted recoater compared to an abrupt transition. Also, a homogenization heat treatment (24 h at 1032 °C) was examined. Finally, a design implementation was fabricated featuring a functionally graded material transition from IN718 to SS316L.

3. Results and discussion

3.1. Parameter derivation for single scan tracks

Processing conditions are converted to linear energy density defined as the ratio of laser power, P, and scan velocity, v, while the amount of interaction is quantified by the dilution ratio defined as the ratio of the melt pool depth, and the sum of the melt pool depth and track height, see inset Fig. 2. The figure shows dilution ratio for single scan tracks of IN718 powder on a SS316L build plate in black and vice versa for SS316L on IN718 in grey. The figure insets show exemplary cross-sectional micrographs of fabricated scan tracks by optical microscopy. Liquid Marangoni flow effects within the melt pool are characteristic of laser melting processes; hence, interaction with the dissimilar substrate material is observed.

Standard IN718 processing parameters are presented as the baseline ($P = 225$ W, $v = 640$ mm/s). Three repeats were observed and show limited variation in dilution ratio ($\sigma < 0.05$). Rescanning (or remelting) without adding additional powder, slightly lowers the dilution ratio, due to an increase in track height. The inset micrograph also suggests much better material mixing compared to the baseline in which solidified convective flow patterns are clearly visible. Increasing the energy density, by either decreasing scan speed ($v = 512$, 425 and 378 mm/s) or increasing laser power ($P = 280$, 338 and 380 W), shows two similar trends with a constant offset. At higher laser power the melt pool depth increased significantly due to the keyholing effect compared to other parameter settings, resulting in a higher dilution ratio.

For processing SS316L powder a lower energy density compared to IN718 is prescribed. The resulting dilution ratios are however generally higher, as shown in Fig. 2 by the grey markers. In all cases, the width of the melt pool was similar, around 160 µm. Hence, the higher dilution ratios can be attributed to dissimilar material properties and hence the order of deposition; e.g., thermal conductivity of SS316L is about 50% and 33% higher than that of IN718 for the solid and liquid state, respectively. Therefore, heat is more easily distributed through the initial melt pool. Moreover, IN718 has a lower melting temperature than SS316L allowing easier penetration. Other effects, such as the surface tension (higher for IN718) and absorptivity (higher for IN718) also affect melt pool shape and track height.

3.2. Elemental diffusion in single scan tracks

Elemental diffusion could best be observed by tracking iron and nickel elements. Transitioning from IN718 to SS316L, the nickel concentration drops from 51wt% to 10wt%, while the iron concentration increases in an opposite trend from 18wt% to 67wt% according to the nominal material compositions.

Fig. 3 shows the nickel concentration relative to the build plate for processing IN718 powder on a SS316L build plate. In all cases, the original 51wt% of nickel in IN718 was not observed indicating that the entire melt pool was mix with material from the build plate. Baseline processing conditions led to large oscillations in material mixing, which can also be observed from the solidified flow pattern in the inset micrograph. Rescanning shows excellent mixing above the build plate but at an elevated plateau; hence, compared to the other process conditions, less material exchange with the substrate occurs. At higher energy density, better mixing with the substrate occurs, as nickel concentrations are distinctively lower compared to the baseline and rescanning conditions, and drop from about 20−25wt% to the final 10wt%. Finally, the penetration depth of IN718 elements into the SS316L build plate are similar, about 100 µm, and for the higher power setting slightly deeper in line with afore dilution ratio results.

The reverse order of deposition (SS316L onto IN718) showed similar results. Nickel and iron concentrations transition similarly in

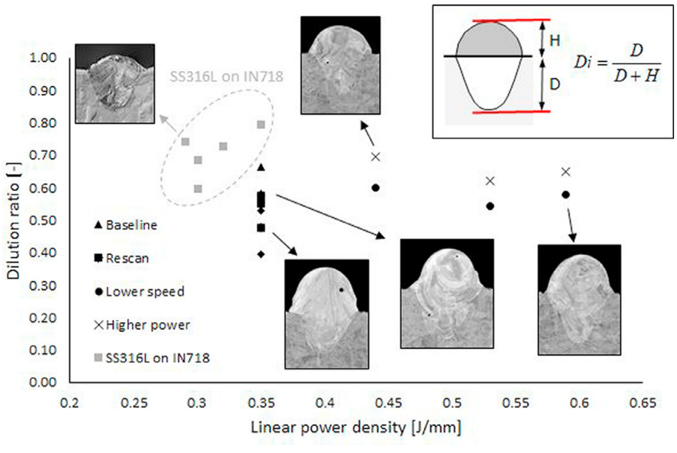

Fig. 2. Dilution ratio, as defined in inset, for single scan tracks of IN718 on SS316L (black) and SS316L on IN718 (grey); micrographs show optical microscopy results.

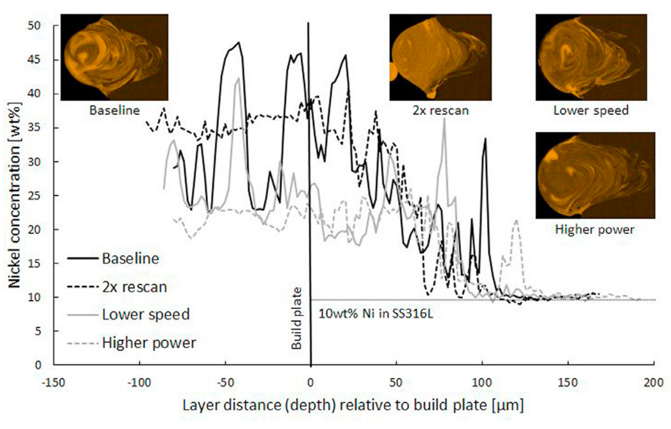

Fig. 3. Element diffusion by nickel concentration through single scan track.; micrographs show SEM and EDX results.

Please cite this article as: W.W. Wits and E. Amsterdam, Graded structures by multi-material mixing in laser powder bed fusion, CIRP Annals - Manufacturing Technology (2021), https://doi.org/10.1016/j.cirp.2021.03.005

opposite trends. At the highest energy density, where the highest dilution was observed, also the best mixing was observed. In this case, the nickel concentration never dropped below 40wt%, while the original SS316L only has 10wt% of nickel and hence the 30wt%-point difference must be brought up from the substrate.

3.3. Hatch scans and interface properties

Next to single (contour) line scans, hatch scans are equally important in LPBF. Similar to the above, both orders of material deposition were examined. Fig. 4(a and b) shows results for each material configuration for a single layer build. Overall, a good metallurgical interface and bond were observed. Melt pool depths remain constant around 100 µm and adjacent line scans touch at a depth of around 50 µm below the surface indicating good adhesion to the previous layer. For IN718 dilution ratios between 0.5 and 0.7 were observed comparable to the single line scan results with higher energy density resulting in distinct higher ratios. Also, for SS316L the average dilution ratio remains similar at 0.7.

Fig. 4(c and d) shows the material interface between IN718 and SS316L for a multi-layer build. The melt pool contours deepen to about 100 µm below the surface for the baseline process parameters. At higher energy density (P = 338 W and v = 640 mm/s), melt pool depths almost double, due to the higher overall energy input compared to a single-layer build, and introduce more material mixing. Contours of sequential melting on top of the previous layer(s) can be observed. The average layer height was in both cases approximately 51 µm and in line with deposited layer thicknesses. Only for rescanning a higher average layer height was observed (66 µm), due to material redistribution in perpendicular, scan line direction.

At the material interface, circular pores up to 10 µm in diameter due to entrapped gas, could be observed. Some small lack-of-fusion defects were seen most notably at higher energy density due to the deeper penetration; however, no cracking was observed.

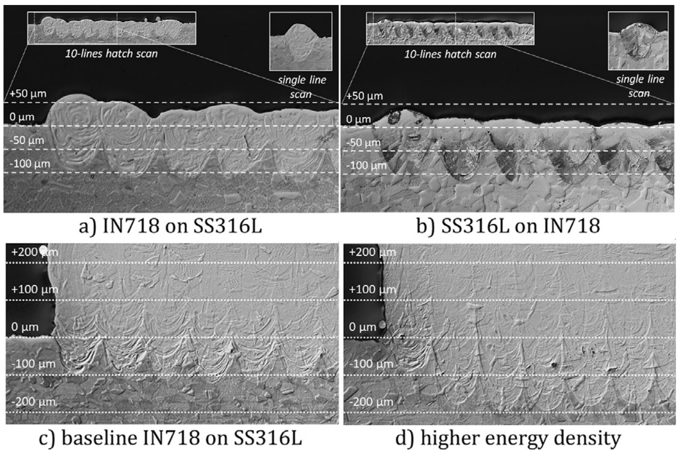

Fig. 4. The interaction of hatched line scans showing the distinct behaviour when depositing a single layer of IN718 on SS316L (a) and the reciprocal arrangement of SS316L on IN718 (b), and the extend of the fusion zone into the SS316L build plate for ten-layer hatch scanning using baseline (c) and higher linear energy density (d).

3.4. Multi-layer elemental diffusion

For the multi-layer builds, elemental diffusion was analysed in a similar fashion to the afore single scan track. Nickel and iron concentrations continue to follow opposite trends. For baseline and rescan conditions, elemental diffusion continued through multiple layers up to approximately 250 µm above the build plate, as shown in Fig. 5 by the black lines. At higher energy density (grey lines), melt pools are deeper and likely remain liquid for longer time. Hence, convective mixing and better elemental diffusion is possible, as is observed from Fig. 5. In this case, between 300 and 450 µm above the build plate a constant plateau is observed indicating good mixing between those layers. In fact, when using higher power even in the tenth and top layer 5wt%-point of nickel concentration was still lacking due to efficient grading with the layers underneath.

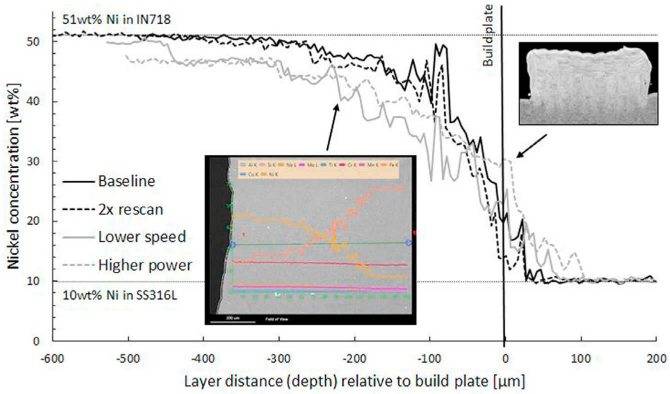

Fig. 5. Elemental diffusion by nickel concentration through a ten-layer build.

As shown in Fig. 4(c and d), at higher energy density the melt pool penetrates deeper into the build plate. This also resulted in better mixing below the surface as demonstrated in Fig. 5 by the grey lines and again most notable at higher power. For a gradual material transition, stretching the diffusion zone is advantageous. To this end, processing at a higher energy density at the material interface seems fitting. There is however a trade-off with the aforementioned increase in lack-of-fusion defects. As a compromise, a ten-layer transition zone consisting of a specific alternating material deposition sequence was explored.

3.5. Gradual transition by alternating material deposition

A more gradual transition zone for grading from material A to B was fabricated in bimetallic cubes using the adapted recoater (see Fig. 1) following a specific layer sequence, as schematically depicted in Fig. 6. The cubes were fabricated following baseline setting for IN718 and varying settings for SS316L: P = 175, 210, 225 and 225 W, and v = 550, 700, 640 and 550 mm/s, for Cubes #1 to #4, respectively. Compared to afore-used techniques and prior work in which an abrupt material change is used, the present technique gives a smoother transition without the necessity to process at higher energy density. This reduces the risk of porosity and cracking.

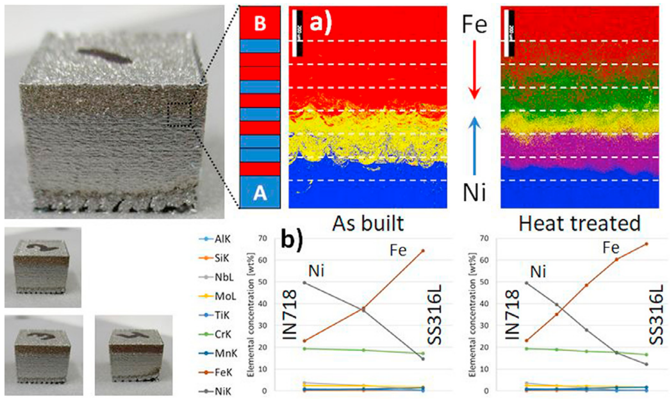

Fig. 6. Bimetallic cubes with alternating material layers in the transition zone; EDX spectra (a) show material phases in different colours for as-built and heat-treated conditions (dashed white lines indicate 100 µm distance) including elemental concentration crossover for nickel and iron (b).

The bottom section of the bimetallic cubes, as shown in Fig. 6, is made from IN718 (material A), the top section is made from SS316L (material B) and a ten-layer alternating material transition zone sits in between. EDX elemental spectra of the transition zone are shown in as-built and heat-treated conditions in Fig. 6(a). The SS316L phase with relatively high iron (Fe) concentration is depicted in red, while the IN718, high on nickel (Ni), is shown in blue. The dashed white lines indicate a distance of 100 µm.

The elemental spectra indicate a gradual transition from IN718 to SS316L over approximately 500 µm. Using optical microscopy, a gradual transition of the microstructure was observed even before heat treatment, which was extended post heat treatment and gave rise to the formation of new phases. The material interface shows good metallurgical bonding as a result. In as-built condition melt pool contours of each line scan are still clearly observable and one intermittent phase (depicted in yellow) is present. Typical of this intermittent phase is that nickel and iron concentrations are almost equal here at 37wt%.

Homogenization heat treatment enhances elemental diffusion resulting in a smooth material transition without a distinct interface. Elemental concentration changes are even more gradual and melt pool contours are no longer visible. In this case, EDX spectra show three intermittent phases (depicted in purple, yellow and green). Compared to an abrupt material change, which shows a nonlinear trend (see Fig. 5), alternating material layers in the transition zone in all cases led to a nearly linear change in elemental concentration indicative of a gradual transition.

Cracking near the interface was observed, similar to the observations reported in literature [13,14]. For both as-built and heat-treated conditions, cracks were observed in the 150 µm zone above the yellow region of Fig. 6, where iron concentration exceeds nickel. As process parameters are optimized for single-material SS316L of which the thermal conductivity is higher than that of IN718, confined liquid melt pool temperatures will likely be higher. Higher thermal stresses induced by larger thermal gradients during re-solidification above the less ductile IN718 may explain the observed cracking. Future work to prevent this should target optimized process parameters for these 3–4 layers above the elemental crossover.

3.6. Design implementation

To demonstrate a possible design implementation, a multi-material heat exchanger was designed and built. Nickel-based superalloys such as IN718 excel in high-temperature strength. However, SS316L has merits at cryogenic temperatures, has higher ductility and is a cost-effective material compared to IN718. In a functionally graded part, material may be placed where needed based on design requirements. This is demonstrated in Fig. 7, in which a material transition is designed approximately midway within the heat exchanger. Two multi-material heat exchangers with a cutaway to show the internal features were fabricated.

The heat exchangers were built using a similar strategy to bimetallic Cubes #1 and #4. The bottom part is made from IN718 and the top part is made from SS316L. The transition zone was fabricated using the same ten-layer alternating material sequence as shown Fig. 6.

Fig. 7. Multi-material heat exchanger functionally graded from IN718 (bottom) to SS316L (top) shown after homogenization heat treatment.

Both heat exchangers were fabricated successfully. In as-built condition, three distinct sections are observable: an IN718 section, a transition zone and a SS316L section. After homogenization heat treatment however, just the two material sections remain discernible, as shown in Fig. 7. All in all, the possibility of creating complex geometries including a gradual material transition by LPBF processes is demonstrated, which exploits the process parameter derivation discussed earlier in this paper.

4. Conclusions

IN718 and SS316L were mixed and successfully bonded by LPBF. Material mixing and elemental diffusion were studied for a range of process conditions. Through the use of an adapted material feeder system it was possible to deposit two materials and directly alternate material layers in one build. Evaluation of the fusion layers at the interface between material types indicates that a graduated region is created associated with liquid state mixing and diffusion. This work also highlights the 'directionality' or order of deposition. Distinct parameters are required when transitioning from material A to B as compared to vice versa. The microstructure of the material interface is consistent with conventional scanning strategies associated with LPBF. A smooth and gradual material transition was observed following an alternating material layer sequence at the interface, although further adaptation of scanning strategies is required in order to develop optimised approaches.

Declaration of Competing Interest

None.

Acknowledgements

The Netherlands Aerospace Centre (NLR) is kindly recognized for hosting Dr. Wits in the Aerospace Vehicle Structures Technology group for his multi-material AM research sabbatical.

References

[1] Gibson I, Rosen DW, Stucker B (2015) *Additive Manufacturing Technologies*, Springer, Boston (MA), US.
[2] Schmidt M, Merklein M, Bourell D, Dimitrov D, Hausotte T, Wegener K, Levy GN (2017) Laser based additive manufacturing in industry and academia. *CIRP Ann.* 561–583. 66/2.
[3] Bourell D, Kruth JP, Leu M, Levy GN, Rosen D, Beese AM, Clare AT (2017) Materials for additive manufacturing. *CIRP Ann.* 659–681. 66/2.
[4] Vock S, Klöden B, Kirchner A, Weißgärber T, Kieback B (2019) Powders for powder bed fusion: a review. *Prog. Addit. Manuf.* 4:383–397.
[5] Bandyopadhyay A, Heer B (2018) Additive manufacturing of multi-material structures. *Mater. Sci. Eng.* 129:1–16.
[6] Wits WW, De Smit M, Al-Hamdani K, Clare AT (2019) Laser powder bed fusion of a Magnesium-SiC metal matrix composite. *Procedia CIRP* 81:506–511.
[7] Demir AG, Previtali B (2017) Multi-material selective laser melting of Fe/Al-12Si components. *Manuf. Lett.* 11:8–11.
[8] Gu H, Wei C, Li L, Han Q, Setchi R, Ryan M, Li Q (2020) Multi-physics modelling of molten pool development and track formation in multi-track, multi-layer and multi-material SLM. *Int. J. Heat Mass Transf.* 151:119458.
[9] Bai Y, Zhang J, Zhao C, Li C, Wang H (2020) Dual interfacial characterization and property in multi-material selective laser melting of 316L stainless steel and C52400 copper alloy. *Mater. Charact.* 167:110489.
[10] Tan C, Wang D, Ma W, Zhou K (2021) Ultra-strong bond interface in additively manufactured iron-based multi-materials. *Mater. Sci. Eng.* 802:140642.
[11] Koopmann J, Voigt J, Niendorf T (2019) Additive manufacturing of a steel–ceramic multi-material by selective laser melting. *Metall. Mater. Trans. B*: 1042–1051. 50/2.
[12] Zhou Y, Zhou X, Teng Q, Wei QS, Shi YS (2015) *Investigation on the Scan Strategy and Property of 316L Steel-Inconel 718 Functionally Graded Materials Fabricated by SLM*, Solid Freeform Fabrication Symp, Austin (TX), USA700–707.
[13] Mei X, Wang X, Peng Y, Gu H, Zhong G, Yang S (2019) Interfacial characterization and mechanical properties of 316L stainless steel/inconel 718 manufactured by SLM. *Mater. Sci. Eng.* 758:185–191.
[14] Chen WY, Zhang X, Li M, Xu R, Zhao C, Sun T (2020) Laser powder bed fusion of Inconel 718 on 316 stainless steel. *Addit. Manuf.* 36:101500.

Please cite this article as: W.W. Wits and E. Amsterdam, Graded structures by multi-material mixing in laser powder bed fusion, CIRP Annals - Manufacturing Technology (2021), https://doi.org/10.1016/j.cirp.2021.03.005